Improved modelling of fatigue loads in wind farms under non-neutral ABL stability conditions

G.C. Larsen[1], S. Ott[1], T.J. Larsen[1], K.S. Hansen[1] and A. Chougule[2]

[1] Technical University of Denmark, Department of Wind Energy
[2] University of Agder, Department of Engineering Sciences

E-mail: gula@dtu.dk

Abstract. The purpose of this study is improve the predictive capability of the DWM model generalized to non-neutral atmospheric boundary layer (ABL) conditions in general and under *stable ABL stratification* in particular. The emphasis is on *rotating* wind turbine components, and the model improvement in focus is intimately linked to a newly developed *refinement of the classic Monin-Obukhov theory*, which, for stable ABL stratification, primary results in less pronounced mean wind shear outside the surface layer, where most modern wind turbines are operating. The model improvements are validated against a huge set of full-scale data, which allows for a one-to-one comparison of wind turbine load simulations and measurements conditioned on ABL stability conditions.

1. Introduction

For wind farm (WF) *production* estimation *stationary* WF flow field modeling as provided by e.g. full CFD RANS models or fast linearized CFD RANS models [1] may suffice. However, for *load estimation* of wind turbines (WT's) exposed to wake affected inflow conditions, a *non-stationary* WF flow field description is inevitable. Insisting on models reflecting the *basic physics* of the problem, and considering direct numerical simulation (DNS) precluded due to its excessive computational demand, we are thus left with either high-fidelity CFD LES actuator disc or line a type of approaches or, alternatively, the medium-fidelity Dynamic Wake Meandering (DWM) [2], [3] type of model approach. CFD LES models must – like the DWM model – be linked to an aeroelastic model of each and every WT in a WF to provide a complete picture of the load conditions inside a WF for all design load cases. This is extremely CPU demanding and considered unrealistic for design purposes even with the capacity of nowadays very powerful state-of-the-ark super computer clusters. This challenge is further enhanced when including ABL stability as an additional design load case dimension and/or considering optimization of WF layout.

Being a medium-fidelity approach the DWM model offers significant savings in CPU-demands compared to the above mentioned non-stationary CFD alternatives, and it thereby facilitates detailed WF production/load design simulations to be conducted even when including the extra design load case dimension constituted by ABL stability. The "classic" (i.e. associated with neutral ABL conditions)

DWM model is well established and about to be included in the revised IEC standard as a recommended practice. The model has been extensively validated both *directly* against full-scale wake affected flow measurements [5], [6], [7] and *indirectly* [8], [9] by using DWM together with the aeroelastic code HAWC2 [10] to compare predictions of WT production and loading with full-scale WF data.

In [9] a huge scatter in the measured load data was observed, and to investigate whether at least part of this scatter can be attributed to ABL stability effects, the DWM model was generalized to *non-neutral* ABL stability conditions [13], [14]. The capability of the generalized DWM model was subsequently investigated using the same set of full-scale WF data in [23], [24]. These studies have demonstrated the importance of ABL stability regarding *fatigue* loading of WTs operating in WF conditions. For fatigue load prediction of *non-rotating* WT components, the validation of the generalized DWM model against the full-scale load data was fully satisfactory. For the investigated *rotating* WT component (i.e. the blade), however, some deviations between measurements and predictions were seen.

The purpose of the present study is therefore to further improve the generalized DWM model with special emphasis on its predictive capability regarding *rotating* WT components, as well as to get further *fundamental* - qualitative and quantitative - *insights* in ABL stability effects on WT loading in WF's.

The paper is structured as follows. First the generalization of the DWM model to non-neutral ABL conditions is briefly described in Section 2. Then follows in Section 3 a description of the impact of non-neutral ABL conditions on the vertical mean wind speed profile, which is a significant load contributor to the fatigue loading of WT blades under stable ABL conditions. Section 4 describes the Lillgrund case study, and in Section 5 results from comparing model simulations with the Lillgrund full-scale measurements are presented and discussed. Finally, conclusions are drawn in Section 5.

2. DWM for non-neutral conditions

The core of the DWM model is a *split of scales* in the wake affected flow field, with large turbulence scales being responsible for stochastic *wake meandering* and small scales being responsible for wake *attenuation* and *expansion* in the meandering frame of reference as caused by turbulent mixing [2]. Thus, the DWM model essentially assumes that the transport of wakes in the ABL can be modeled by considering the wakes to act as passive tracers driven by a combination of large-scale turbulence structures and a mean downstream advection velocity, adopting the Taylor hypotheses [4]. This basic split in scales further facilitates generalization of the DWM model to non-neutral ABL stability conditions in a simplistic way, as ABL stability is known primary to affect the low wave number turbulence regime.

The large scale turbulence structures, used to describe wake dynamics in the DWM model, are traditionally provided by a fast Navier-Stokes (NS) consistent turbulence model [11] which, however, assumes *neutral* ABL stability and thereby neglect the effects of buoyancy on turbulence production and thus turbulence characteristics. As ABL stability mainly affects the large scale turbulence structures [4], the effect of buoyancy on wake meandering cannot be neglected. In addition, the significance of buoyancy effects on small turbulence structures relevant for wake deficit expansion and attenuation in the meandering frame of reference must be clarified. The crucial question in this respect is whether the effect of buoyancy can be "decomposed" in analogy with the description of wake dynamics.

The starting point is the following fundamental conjecture launched in [12]: *In a wake context, ABL stability affects primary wake meandering driven by large (lateral and vertical) turbulent scales, whereas wake expansion in the meandering frame of reference is a second order effect only.* This conjecture has been investigated for a variety of stability conditions in [13] and [14], respectively. Based on full-scale LiDAR and sonic measurements as well as detailed numerical simulations the wake affected flow field behind a 500kW turbine was examined with focus on both organized wake deficit flow structures (resolved in the meandering frame of reference) and wake dynamics. These extensive investigations have justified the above stated conjecture, and we will therefore generalize the applicability of the DWM model to non-neutral ABL stability regimes by adopting this conjecture.

For consistency, we need a generalization of the classical spectral tensor to the non-neutral regime. Such a model has been developed and validated against full-scale data in [15], [16] and [17]. Being a

generalization of the classical Mann spectral tensor, this model share some of the basic features of the Mann spectral tensor (i.e. the *linear* vertical mean wind speed profile and the eddy life time model), but includes in addition a *linear* vertical temperature profile as well as buoyancy terms from the linearized NS equations used in the Rapid Distorsion approach. The inclusion of buoyancy comes with a cost of two additional input parameters. For consistency reasons, the generalized spectral tensor is used to model both the large- and small scale ABL turbulence used with the DWM model, although the primary effect on the turbulence structure is on the big spatial scales (i.e. the low wave number regime).

3. Vertical mean wind speed profile for non-neutral conditions

Apart from turbulence intensity and turbulence structure, non-neutral ABL stability conditions also affect the vertical *mean wind speed profile* and the *wind veer* significantly - especially in the stable regime. This is not essential for fatigue loading of non-rotating WT components as e.g. the tower, but for rotating WT components like blades, especially the shear profile is of crucial importance. In the present study we will neglect the effect of ABL stability on the wind veer.

The vertical mean wind speed profile is stability dependent through the impact of buoyancy on mixing in the ABL layer – in stable conditions with little/suppressed mixing the gradient of vertical mean wind speed profile tend to increase, whereas in unstable conditions, with increased mixing, the vertical mean wind speed profile tend to become more uniform.

Within the surface layer the *Monin-Obukhov (M-O) scaling theory* has proven very successful and is widely used. Adopting the physically consistent logarithmic profile for the neutral case and neglecting the influence of boundary layer height, the M-O formulation of the *non-neutral* vertical mean wind speed profile, U, may be expressed as [4]

$$U_{MO}(z, z_0, L_M) = \frac{u_*}{\kappa}\left[Ln\left(\frac{z}{z_0}\right) - \psi_m\left(\frac{z}{L_M}\right)\right], \tag{1}$$

where u_* is the friction velocity, z_0 is the roughness length, L_M is the M-O scaling length, and $\kappa = 0.41$ is the von Karman constant. The celebrated stability function, ψ_m, has unstable- and stable branches, respectively.

The vertical mean wind speed profile may, under *unstable conditions*, be formulated as [4] , [21]

$$U_{MO}(z, z_0, L_M) = \frac{u_*}{\kappa}\left[Ln\left(\frac{z}{z_0}\right) - Ln\left[\frac{1+x^2}{2}\left(\frac{1+x}{2}\right)^2\right] + 2Atan(x) - \frac{\pi}{2}\right];$$
$$-2 \le z/L_M < 0; \tag{2}$$
$$x = \left(1 - 16\frac{z}{L_M}\right)^{1/4}$$

The analog expression for the vertical mean wind speed profile under *stable conditions* is given by [4]

$$U_{MO}(z, z_0, L_M) = \frac{u_*}{\kappa}\left[Ln\left(\frac{z}{z_0}\right) + 5\frac{z}{L_M}\right]; 0 < z/L_M \le 1 \tag{3}$$

Classic M-O scaling is in principle limited to the surface layer. This has been challenged in a recent Danish study [25], where a thorough investigation of 3 Danish offshore sites (Horns Reef; Nysted; and Læsø) *outside* the surface layer has been conducted. The investigation demonstrates that mean wind speeds in *unstable* cases are remarkably well predicted by the classic surface layer M-O similarity theory even outside the surface layer. In *stable* cases, however, some large over-predictions were observed, especially for low mean wind speeds under strongly stable conditions (cf. Figure 1a).

The failure of conventional M-O theory in (some) stable cases has led to the development of an extended version of the M-O theory, in which a correction to the classic M-O theory for *stable* conditions is re-formulated. For derivation of the extended M-O theory we refer to [25]. The developed extended M-O theory has been validated against full-scale meteorological observations. Convincing agreement

between model predictions and full-scale data has been demonstrated in altitude the regime ranging from 62m and up to 900m using data from 3 Danish offshore sites as well as from the German Fino platform, and it is concluded that the model is behaving surprisingly well even for heights elevated high above the surface layer (cf. Figure 1b).

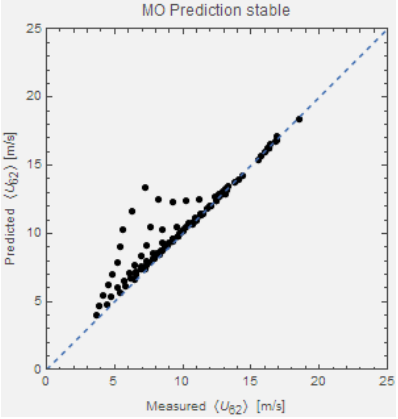

Figure 1a. Predicted *classic* M-O vs. measured values of bin averaged U_{62}. Horns Reef at 62m altitude.

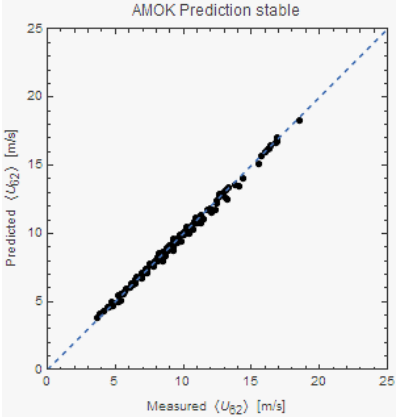

Figure 1b. Predicted *extended* M-O vs. measured values of bin averaged U_{62}. Horns Reef at 62m altitude.

To describe the extended M-O theory we re-write eq. (3) as

$$\begin{aligned} U_{MO}(z, z_0, L_M) &= \frac{u_*}{\kappa}\left[Ln\left(\frac{z}{z_0}\right) - \psi_m^{(s)}\left(\frac{z}{L_M}\right)\right] \\ &= \frac{u_*}{\kappa}\left[Ln\left(\frac{z}{L_M}\right) - Ln\left(\frac{z_0}{L_M}\right) - \psi_m^{(s)}\left(\frac{z}{L_M}\right)\right] \end{aligned} \tag{4}$$

where upper index '(s)' indicates the stable branch of the on the stability correction function. Introducing non-dimensional variables

$$\tilde{z} = \frac{z}{L_M}\ ; \quad \tilde{z}_0 = \frac{z_0}{L_M} \tag{5}$$

eq. (4) may be reformulated as

$$U_{MO}(\tilde{z}, \tilde{z}_0) = \frac{u_*}{\kappa}\left[Ln(\tilde{z}) - Ln(\tilde{z}_0) - \psi_m^{(us)}(\tilde{z})\right] \tag{6}$$

The extended M-O theory, developed in [25], expresses the vertical mean wind speed profile under *stable conditions* as

$$U_{EMO}(\tilde{z}, \tilde{z}_0, \mu) = \frac{U_{MO}(\tilde{z}, \tilde{z}_0)}{\sqrt{1 + b\tilde{z}^2/\mu}} \tag{7}$$

with μ being the Monin-Kazanski parameter (the non-dimensional Coriolis parameter) defined by

$$\mu = \frac{u_*}{fL_M} \tag{8}$$

where f is the Coriolis parameter defined by

$$f = 2\Omega\ Sin(\varphi) \tag{9}$$

Ω is the rotation rate of the Earth, and φ is the latitude. At the Lillgrund location $f = 1.914 \times 10^{-5}$Hz.

4. The Lillgrunden case

The Lillgrund WF consists of 48 Siemens SWT-2.3-93 WT's. The layout of the WF is shown in Figure 2 along with the location of the Drogden light tower.

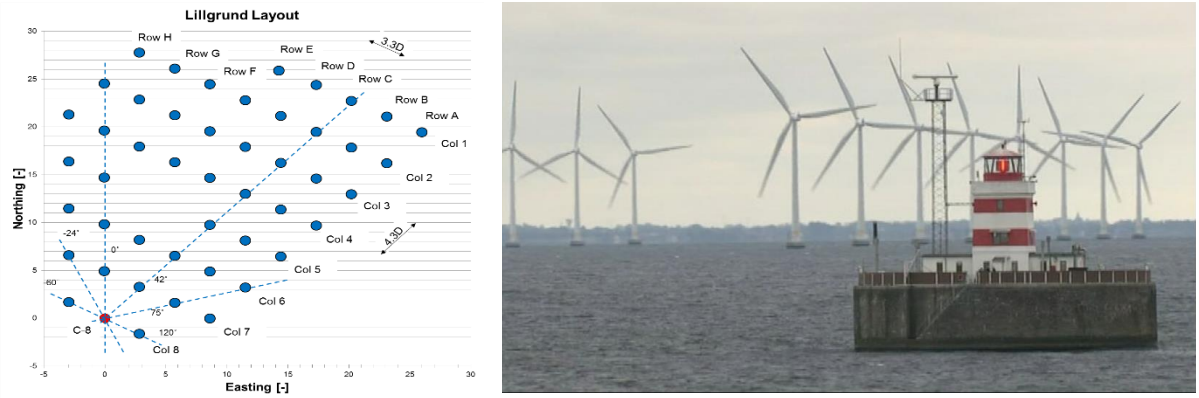

Figure 2. Layout of the Lillgrunden WF with the instrumented WT C-8 marked. Distances are non-dimensioned with the rotor diameter**.** Also shown is Drogden light tower located WNW of the WF. The distance between WF and the light tower roughly corresponds to a characteristic scale of the WF.

Whereas the Egmond aan Zee WF, previously investigated in [8], is characterized by a "conventional" WT inter spacing, the layout of the Lillgrund WF is characterized by very small WT inter spacing's – i.e. down to 3.3 D. This makes the Lillgrund WF especially interesting and challenging as a wake-load validation case, because the close spacing magnifies wake generated load effects compared to more traditional spaced WF's.

4.1. Measurements

One of the Lillgrund WT's (C-8) is instrumented with strain gauges resolving respectively the blade root flap bending moment, two main shaft bending moments and the tower base for-aft bending moment. These measurements have been made available by Siemens Wind Power, and they constitute probably one of the most comprehensive sets of wake affected wind turbine load measurements ever recorded. The measurement period extends from 2008-06-03 to 2013-03-19 – i.e. over a period of almost 5 years. In addition to these high-frequency data, WT SCADA data (pitch setting, rotational speed and electrical power) were available for the WF WT's during the measuring period.

Unfortunately no meteorological mast data was available within the recording period, but as the WT power and pitch angle are directly correlated with the inflow wind speed, the ambient undisturbed wind speed has been determined as based on power and pitch angle recordings for corner placed WT's located in free inflow conditions. A similar philosophy was used for estimating the ambient undisturbed wind direction, which was determined from nacelle orientations of corner placed WT's. These nacelle orientations were initially calibrated against power deficit polar's constrained to directions, where wake losses were dominated by the closest neighboring WT's. To facilitate stability classification, meteorological data from the nearby Drogden light tower was offered for the investigation. This light tower is located a few kilometers WNW of the WF, and with the distance being of the same order of magnitude as the extension of the WF, the light tower meteorological data are deemed applicable for stability classification of the WF structural data. The data set holds approximately 15.600 hours of measurements covering the period 2008–2013. Like the structural data, the light tower data are organized as 10-minute recordings, and 10-minute mean values of wind speed and temperature at 22m altitude as well as water temperature 1m below mean sea level (MSL) was available.

As for the structural data, full polar load cases, associated with normal WT operation, are available for mean wind speeds ranging from 6m/s to 16m/s. Data binning in 3 dimensions – mean wind speed; mean wind direction; and ABL stability class – is quite demanding and requires a huge set of data. The desire of smallest possible bins has to be balanced against sufficient 'data population' of each individual

bin, and in the end it was decided to use 2m/s bins for the mean wind speed and 4 deg. bins for the wind direction. The ABL stability was classified according to Table 1, which is obtained from the suggested stability classification in [26] by collapsing these stability classes into only 3 classes.

Table 1. ABL **s**tability classification in terms of Monin-Obukhov length L_M.

Description	Stability identifier	Condition
Unstable	-2	-200m < L_M < -50m
Neutral	0	200m < | L_M|
Stable	2	10m < L_M < 200m

The blade root flap moments and the tower bottom for-aft moments have been post processed to fatigue equivalent moments using the Palmgren-Miner [18] approach and subsequently normalized with the respective fatigue equivalent moments associated with an inflow wind speed of 9m/s – i.e. here represented by mean equivalent moments associated with the velocity bin [8;10]m/s. Wöhler exponents of 4 and 10 were assumed for the tower and blade composite structures, respectively.

4.2. Simulations

For the DWM/HAWC2 validation study the load response of WT C-8 is simulated for mean wind speeds reflecting the median of the velocity bins defined for the measurements. Measured wind speed dependent turbulence intensities (TI's) are used, reflecting the offshore wind speed dependent "surface" roughness. However, no attempt is done to resolve TI as function of upstream fetch (i.e. direction). Thus, in the mean wind speed regime 6m/s-14m/s a TI of 5.8% is used – gradually increasing to 6.2% at 16m/s.

4.2.1. Mean wind shear

Because site meteorology measurements, facilitating derivation of the site mean wind speed vertical profile, doesn't exists, it was decided to use the IEC offshore wind shear profile as a surrogate for the *neutral* profile in the analysis. The IEC offshore profile is specified in terms of a power exponent α equal to to 0.14 [20]. To recast this profile into the more physically sound log-formulation described in Section 3, we approximated a log-profile to the IEC power law profile. Specifically, the best possible agreement of respectively the power law profile and log profile over the vertical extent of the rotor was requested, and this 'best' fit was defined in terms of minimum least square metric Π. Thus

$$\Pi(z_0) = {U_{hub}}^2 \int_{z_{hub}-R}^{z_{hub}+R} \left[\frac{Ln(z/z_0)}{Ln(z_{hub}/z_0)} - \left(\frac{z}{z_{hub}}\right)^{\alpha} \right]^2 dz \tag{10}$$

where the requested roughness, z_0, are defined the particular value that minimizes Π; viz.

$$\widehat{z_0} = \left\{ \widehat{z_0} \,\middle|\, \Pi(\widehat{z_0}) = \min_{z_0}\{\Pi(z_0)\} \right\} \tag{11}$$

Adopting the roughness defined in eq. (11), the vertical mean wind speed profile for the non-neutral ABL stability conditions was evaluated using eqs. (2) and (7) for the unstable- and the stable ABL regime, respectively.

4.2.2. Turbulence

The coupled DWM-HAWC2 platform [3] requires simulation of three different turbulence fields – a large scale turbulence field dictating the wake meandering, a traditional turbulence field accounting for conventional WT turbulence loading, and an *isotropic* and *inhomogeneous* small scale turbulence field accounting for WT loading caused by wake self-generated turbulence. The wake self-generated turbulence field is assumed to be invariant with respect to the ABL stability condition, and it is simulated using the classic Mann turbulence simulator [11]. The two remaining turbulence fields, which are highly dependent on ABL stability conditions, are generated based on the generalized buoyancy dependent

spectral tensor [15], [16], [17], which degenerates to the classic spectral tensor for neutral stability conditions. In all cases the turbulence fields are simulated as three dimensional fields resolved in suitable Cartesian grid configurations.

The parameters of the buoyancy dependent spectral tensor are, for each stability class, obtained from fitting model auto- and cross spectra to respective spectra obtained from full-scale sonic measurements from the Høvsøre site in Denmark. Data associated with the [8;9]m/s mean wind speed bin were used for the parameter fitting due to the good data coverage. Of the available sonic measurements, it was decided to base the fitting on data from a sonic located at 40m altitude, because this sonic is more likely to be within the surface layer, where L_M is defined, than the sonic's located at higher alternative altitudes (especially for stable stratification). Moreover, the model fitting to data at this altitude seems to slightly to outperform the fits to alternative sonic data.

Except for the turbulence intensity (described by the $\alpha\varepsilon^{2/3}$ parameter of the spectral tensor *when* the remaining parameters have been fixed), it was further decided to adopt the (neutral) turbulence input specifications from the IEC code to [19] mimic the turbulence conditions at the Lillgrund site, where no high-frequency meteorological measurements, as mentioned, are available. The IEC spectral tensor input parameters were originally obtained by fitting the spectral tensor spectra to a target Kaimal spectra [19]. Since we have decided to base the neutral turbulence generation partly on IEC specifications of turbulence tensor input (i.e. turbulence length scale L and eddy life time parameter Γ), the spectral tensor input parameters for neutral conditions do not match the fitted parameter values from the Høvsøre full-scale data. As a consequence, it was decided to scale (L, Γ) for the non-neutral (i.e. diabatic) conditions accordingly, although this approximation might not be completely true. However, it is believed to be a fair approximation – alternatively the neutral case could defined by the directly fitted values for L and Γ at the Høvsøre site, which is just another approximation to the Lillgrund conditions.

5. Results

The results for the blade root equivalent moments and for the tower base for-aft equivalent moments are presented for the investigated ABL stability regimes in Figure 3 and in Figure 4, respectively.

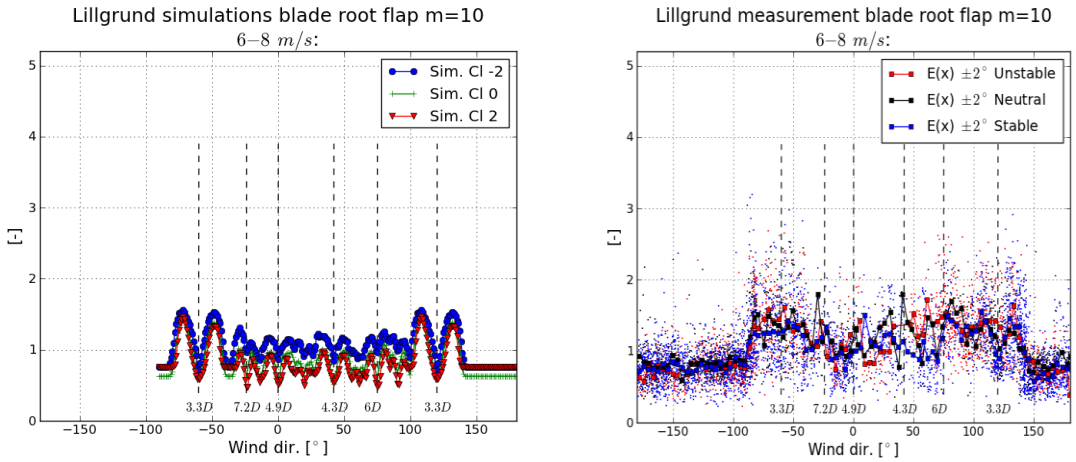

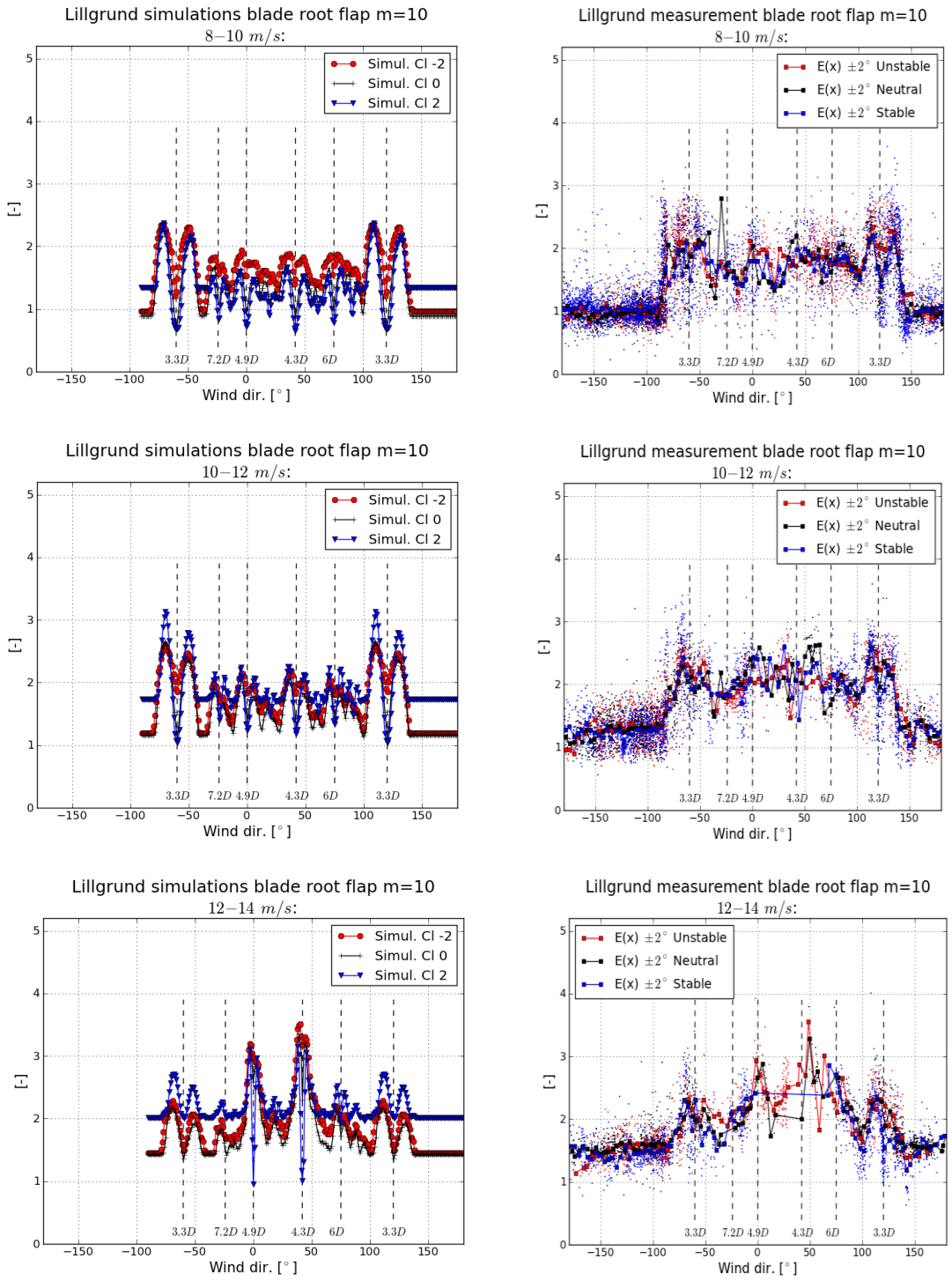

Figure 3: Comparison of measured and simulated blade flap fatigue loads for the C-8 turbine. Solid markers connected by lines in the plots of the measured data represents direction bin specific mean values.

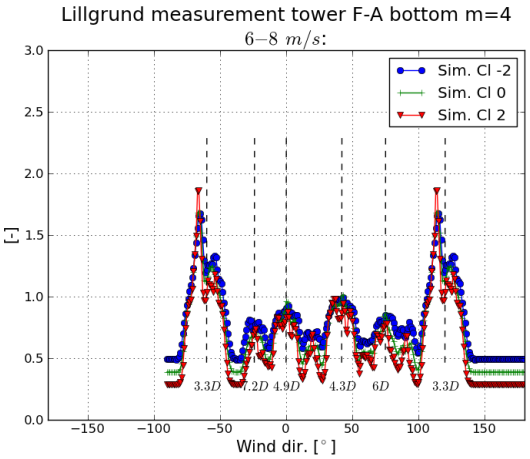
Lillgrund measurement tower F-A bottom m=4
$6-8\ m/s$:
Sim. Cl -2
Sim. Cl 0
Sim. Cl 2
[-]
Wind dir. [°]
3.3D
7.2D
4.9D
4.3D
6D
3.3D

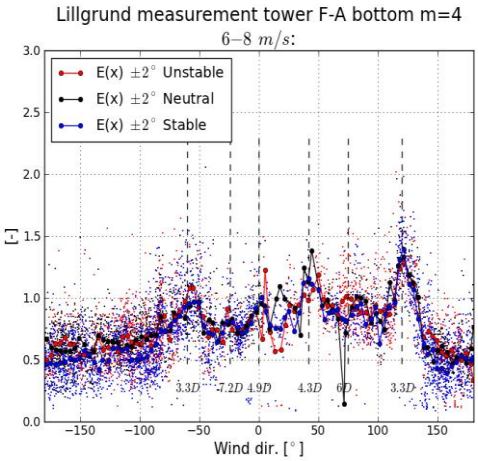
Lillgrund measurement tower F-A bottom m=4
$6-8\ m/s$:
E(x) $\pm 2^\circ$ Unstable
E(x) $\pm 2^\circ$ Neutral
E(x) $\pm 2^\circ$ Stable
[-]
Wind dir. [°]
3.3D
7.2D
4.9D
4.3D
6D
3.3D

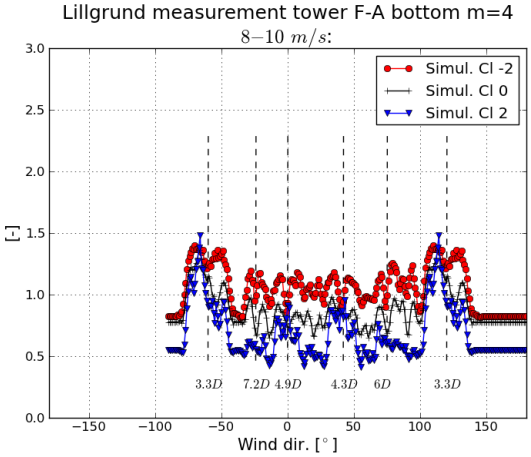
Lillgrund measurement tower F-A bottom m=4
$8-10\ m/s$:
Simul. Cl -2
Simul. Cl 0
Simul. Cl 2
[-]
Wind dir. [°]
3.3D
7.2D
4.9D
4.3D
6D
3.3D

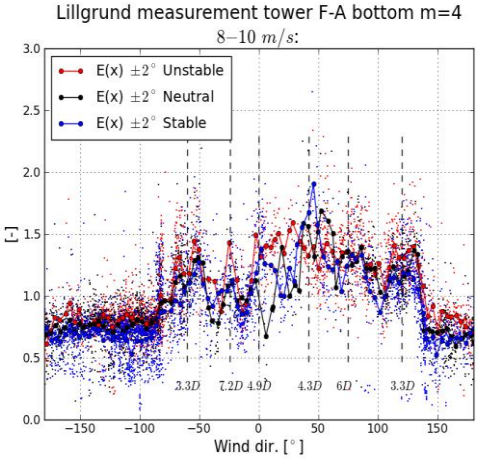
Lillgrund measurement tower F-A bottom m=4
$8-10\ m/s$:
E(x) $\pm 2^\circ$ Unstable
E(x) $\pm 2^\circ$ Neutral
E(x) $\pm 2^\circ$ Stable
[-]
Wind dir. [°]
3.3D
7.2D
4.9D
4.3D
6D
3.3D

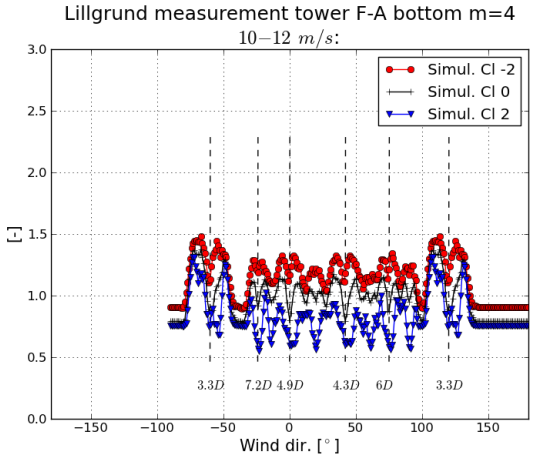
Lillgrund measurement tower F-A bottom m=4
$10-12\ m/s$:
Simul. Cl -2
Simul. Cl 0
Simul. Cl 2
[-]
Wind dir. [°]
3.3D
7.2D
4.9D
4.3D
6D
3.3D

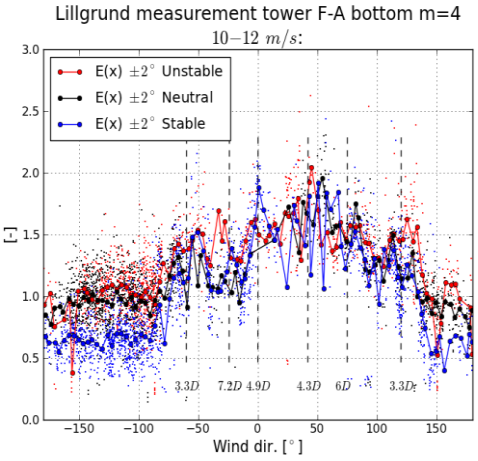
Lillgrund measurement tower F-A bottom m=4
$10-12\ m/s$:
E(x) $\pm 2^\circ$ Unstable
E(x) $\pm 2^\circ$ Neutral
E(x) $\pm 2^\circ$ Stable
[-]
Wind dir. [°]
3.3D
7.2D
4.9D
4.3D
6D
3.3D

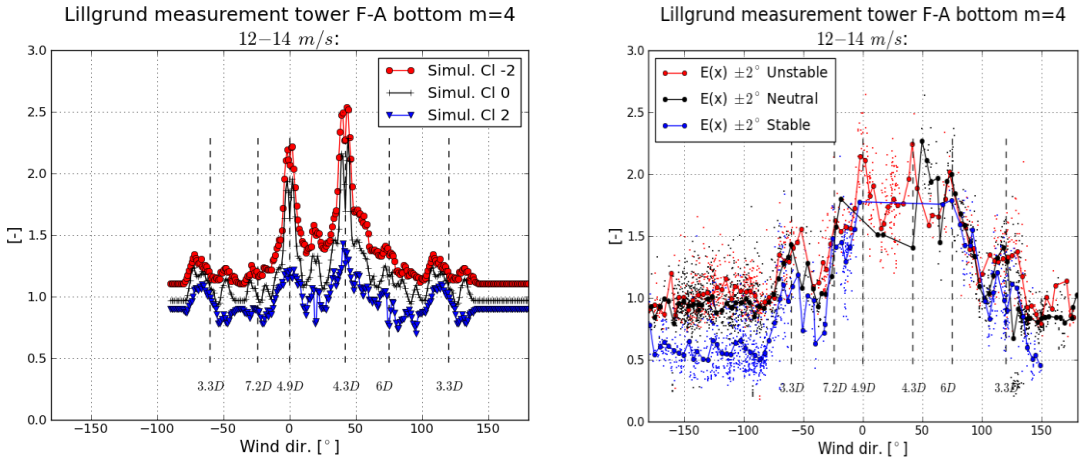

Figure 4: Comparison of measured and simulated tower bottom for-aft fatigue loads for the C-8 turbine. Solid markers connected by lines in the plots of the measured data represents direction bin specific mean values.

For all wind speeds it can be seen that the *tower bottom fatigue bending moments* are largest in unstable and smallest in stable ABL conditions. This is explained by the difference in turbulence intensity associated with the investigated ABL stability conditions, where unstable conditions causes a turbulence level of 9.8%, neutral conditions corresponds to a turbulence level of 6.0%, and stable conditions corresponds to a turbulence level of 1.99%. The measured load levels are in general captured reasonable well by the simulations. However, the difference in fatigue load level caused by ABL stability effects are typically larger under multiple wake inflow situations in the simulations than seen from the measurements.

In the inflow sector 150deg. –180deg. the investigated WT is *not* affected by upstream wakes, and it is thus possible to evaluate the impact from ABL stability on solitary WT loading. When investigating the blade *flapwise fatigue loads* in this free sector, the results are significantly different from the tower fatigue loading. Contrary to tower loading, the blade loads are sensitive to both shear- and turbulence levels, as both cause varying wind speeds over the rotor area. For rotating WT components these are *counter acting effects*, because stable conditions result in large shear and low turbulence intensity and vice versa for unstable conditions. It is seen, that even with the mean wind speed profile modeled based the *extended* M-O theory, the impact from wind speed shear on the blade fatigue loading is still significantly over-estimated. One reason could be the crude classification of ABL stability applied in this investigation, since the M-O correction formulated in eq. (7) is sensitive to the specific ABL stability condition - especially in the *below rated* mean wind speed regime (cf. Figures 1a and 1b). For most wind speeds, it is seen that the fatigue load level 'inside the WF' (i.e. corresponding to multiple wake inflow situations) is quite well predicted.

6. Conclusion

A medium-fidelity DWM/HAWC2 framework for modelling of wind turbine component fatigue loading, when the wind turbines are subjected to wake affected *non-stationary* flow fields under *non-neutral* atmospheric stability conditions, has been developed and demonstrated on full-scale load data from the Lillgrunden WF. Compared to previous studies [23], a newly developed refinement of the classic M-O scaling theory was included in this study to account for un-realistic wind speed shears above the ABL surface layer under (strongly) stable stratification. This has reduced, but not removed, the over-prediction of blade fatigue loading of solitary WT's in (strongly) stable stratification.

A comparative analysis of measured and simulated blade and tower fatigue loads has revealed that ABL stability effects can explain a significant part of the large measurement scatter observed in full-scale data. The study has further gained insight in important load mechanism, and shown that vertical

mean wind speed shear is the dominating fatigue load driver for the rotating WT components in stable ABL conditions, whereas turbulence (including its dictating wake meandering mechanism) is the dominating load driver for tower fatigue loading in general. Similar results were found in [22].

In a future perspective, the mean wind speed veer - also predicted by the extended M-O theory - will be included in the HAWC2/DWM model platform, as well as selected meso-scale effects. Finally, it is considered to consolidate the present Drogden based stability classification with WRF-simulations.

Acknowledgements
Siemens Wind Power has provided the unique set of Lillgrunden load measurements used for this study, which is gratefully acknowledged. Further, the EUDP/ForskEL project "PowerKey - Enhanced WT control for optimized WPP" (64017-0045/12558) is acknowledged for financial support.

References

[1] Ott S, Berg J and Nielsen M (2011). Linearised CFD Models for Wakes, Risoe-R-1772(EN).

[2] Larsen GC, Madsen HAa, Thomsen K and Larsen TJ (2008). Wake meandering - a pragmatic approach. Wind Energy, **11**, pp. 377–395.

[3] Madsen HAa, Larsen GC, Larsen TJ and Troldborg N (2010). Calibration and validation of the dynamic wake meandering model for implementation in an aeroelastic code. Journal of Solar Energy Engineering, **132(4)**: 041014-1–041014-14. DOI: 10.1115/1.4002555.

[4] Kaimal JC and Finnigan JJ (1994). Atmospheric Boundary layer Flows – Their structure and Measurement. Oxford University Press.

[5] Bingöl F, Mann J and Larsen GC (2010). Light detection and ranging measurements of wake dynamics. Part I: one-dimensional scanning. Wind Energy, **13(1)**, pp. 51–61.

[6] Trujillo J, Bingöl F, Larsen GC, Mann J and Kühn, M (2011). Light detection and ranging measurements of wake dynamics. Part II: two-dimensional scanning. Wind Energy, **14** pp. 61–75.

[7] Machefaux E, Larsen GC, Troldborg N, Gaunaa M and Rettenmeier A (2015). Empirical modeling of single-wake advection and expansion using full-scale pulsed lidar-based measurements. Wind Energy, **18**, pp. 2085–2103.

[8] Larsen TJ, Madsen HAa, Larsen GC and Hansen KS (2012). Verification of the Dynamic Wake Meander Model for Loads and Power Production in the Egmond aan Zee Wind Farm. Wind Energy, **16**, pp. 605–624.

[9] Larsen TJ, Larsen GC, Madsen HAa, Thomsen K and Pedersen SM (2015). Wake effects above rated wind speed - An overlooked contributor to high loads in wind farms. Scientific Proceedings, EWEA Annual Conference and Exhibition 2015, pp. 95-99.

[10] Larsen TJ and Hansen AM (2007). How to HAWC2, the Users Manual, Risø-R-1597(EN), Risø National Laboratory - Technical University of Denmark.

[11] Mann J (1998). Wind field simulation**.** Probabilistic Engineering Mechanics, **13**, pp. 269-282.

[12] Larsen GC, Larsen TJ, Mann J, Peña A, Hansen KS and Madsen HAa (2009). The dependence of wake losses on atmospheric stability characteristics. EUROMECH Colloquium 508 on Wind Turbine Wakes 2009, pp. 35–37.

[13] Larsen GC, Machefaux E and Chougule A (2015). Wake meandering under non-neutral atmospheric stability conditions – theory and facts. Journal of Physics: Conference Series (Online), **625**, 012036.

[14] Machefaux E, Larsen GC, Tilman K, Troldborg N, Kelly MC, Chougul A, Hansen KS and Rodrigo JS (2016). An experimental and numerical study of the atmospheric stability impact on wind turbine wakes**.** Wind Energy, **19**, pp. 1785–1805.

[15] Chougule A, Mann J, Kelly MC and Larsen GC (2016). Modeling atmospheric turbulence via rapid-distortion theory: spectral tensor of velocity and buoyancy. Journal of the Atmospheric Sciences, Vol. **74**, Issue 4, pp. 949–974.

[16] Chougule A, Mann J, Kelly MC and Larsen GC (2016). Validation of buoyancy driven spectral tensor model using HATS data. Journal of Physics: Conference Series (Online), Vol. **753**, No. 3, 032038.

[17] Chougule A, Mann J, Kelly MC and Larsen GC (2017). Simplification and Validation of a Spectral-Tensor Model for Turbulence Including Atmospheric Stability. Boundary-Layer Meteorology. https://doi.org/10.1007/s10546-018-0332-z.

[18] Miner (1945) MA. Cumulative damage in fatigue. Journal of Applied Mechanics, 12, pp. 159–164.

[19] IEC 61400-1. Wind turbines—part 1: Design requirements, 2005.

[20] IEC 61400-3. Wind turbines – part 1: Design requirements for offshore wind turbines, 2009.

[21] Paulson CA (1970). The mathematical representation of wind speed and temperature profiles in the unstable surface layer. J. Appl. Meteor., 9, 857-861.

[22] Sathe A, Mann J, Barlas T, Bierbooms WAAM and van Bussel GJW (2013). Influence of atmospheric stability on wind turbine loads. Wind Energy, Vol. **16**, Issue 7, pp. 1013–1032.

[23] Larsen GC, Larsen TJ and Chougule A. (2017). Medium fidelity modeling of loads in wind farms under non-neutral ABL stability conditions – a full-scale validation study. Journal of Physics: Conference Series (Online), **854**, 012026.

[24] Larsen GC, Larsen TJ and Hansen KS (2017). Loads in wind farms under non-neutral ABL stability conditions: A full-scale validation study of the DWM model.International Conference on Future Technologies for Wind Energy, WindTech 2017, 24-26 Oct. 2017, Boulder, United States.

[25] Larsen GC et al. (2016). Impact of atmospheric stability conditions on wind farm loading and production. DTU Wind Energy Report-E-0136.

[26] Gryning S-E et al. (2007). On the extension of the wind profile over homogeneous terrain beyond the surface layer. Boundary-Layer Meteorology **124**, pp. 251–268.